ACS APPLIED MATERIALS & INTERFACES

RESEARCH ARTICLE

www.acsami.org

Enhancement of Field Emission and Photoluminescence Properties of Graphene-SnO_2 Composite Nanostructures

Jijun Ding,[†] Xingbin Yan,[*,†] Jun Li,[†,‡] Baoshou Shen,[†,§] Juan Yang,[†] Jiangtao Chen,[†] and Qunji Xue[†]

[†]State Key Laboratory of Solid Lubrication, Lanzhou Institute of Chemical Physics, Chinese Academy of Sciences, Lanzhou 730000, China

[‡]Graduate University of Chinese Academy of Sciences, 100049 China

[§]School of Science, Lanzhou University of Technology, Lanzhou 730050, China

ABSTRACT:

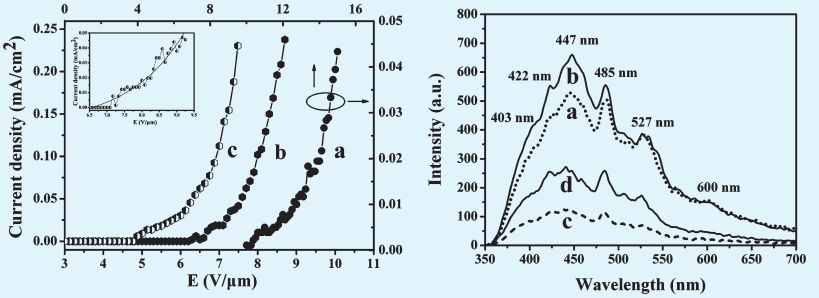

In this study, the SnO_2 nanostructures and graphene-SnO_2 (G-SnO_2) composite nanostructures were prepared on n-Si (100) substrates by electrophoretic deposition and magnetron sputtering techniques. The field emission of SnO_2 nanostructures is improved largely by depositing graphene buffer layer, and the field emission of G-SnO_2 composite nanostructures can also further be improved by decreasing sputtering time of Sn nanoparticles to 5 min. The photoluminescence (PL) spectra of the SnO_2 nanostructures revealed multipeaks, which are consistent with previous reports except for a new peak at 422 nm. Intensity of six emission peaks increased after depositing graphene buffer layer. Our results indicated that graphene can also be used as buffer layer acting as interface modification to simultaneity improve the field emission and PL properties of SnO_2 nanostructures effectively.

KEYWORDS: graphene, SnO_2, electrophoretic deposition, magnetron sputtering, field emission, photoluminescence

1. INTRODUCTION

Field-emission properties of metal oxide nanostructures have been explored extensively.[1] Researchers have also attempted to further improve the field emission properties of various metal oxide nanostructures. Wang et al.[2] reported that highly oriented SnO_2 nanorod arrays have more excellent field emission than SnO_2 films. Wu[3] fabricated Sb-doped SnO_2 and SnO_2 nanowires; he found that the field emission of SnO_2 nanowires was improved by doping Sb. Jang et al.[4] concluded that post-treatment of H_2 exposure can be an available process for improving the field emission properties of various nanowire- or nanorod-based field-emission displays with a high aspect ratio in field emission displays. Tang et al.[5] reported that deposition of Au film or ZnO buffer layer acting as interface modification can also be an effective method to improve field emission properties. The main reason is that Au film or ZnO buffer layer prevent insulative SiO_2 layer from being formed at interface. Meanwhile, deposition of Au film can improve field emission of ZnO nanoarrays more effectively than deposition of ZnO buffer layer. They believed that Au film is an electron-transport material in this process and hence improve electron-transport capability of ZnO nanoarrays.

Graphene possess a 0 eV energy band gap, allowing the electronic properties to vary between those found in a wide gap semiconductor (or insulator) and those of a semimetal.[6] Meanwhile, graphene as a two-dimensional macromolecular sheet of carbon atoms has superior electrical conductivity and mechanical properties,[7] which would make it an excellent electron-transport material in the process of photocatalysis, even more appropriate than C_{60}, polyaniline, graphite-like carbon.[8] Recently, Zhang et al.[9] reported that graphene has a high level of emission currents with a low external electric field. These findings suggest that such a nanomaterial might also be an attractive material for electron-transport material in field emission displays.

Graphene-metal oxide nanocomposite such as graphene-CuO (G-CuO),[10−12] graphene-Co_3O_4 (G-Co_3O_4),[13] graphene-ZnO (G-ZnO),[14−16] graphene-TiO_2 (G-TiO_2)[17−21] and graphene-SnO_2 (G-SnO_2)[22−30] have been prepared by various methods. However, detailed studies on the effect of graphene buffer layers on field-emission properties of SnO_2 have not yet been performed. For these reasons, it is expected that the SnO_2 composite nanostructures with graphene buffer layer would increase the

Received: July 23, 2011
Accepted: October 3, 2011
Published: October 03, 2011

dx.doi.org/10.1021/am2009635 | *ACS Appl. Mater. Interfaces* 2011, 3, 4299–4305

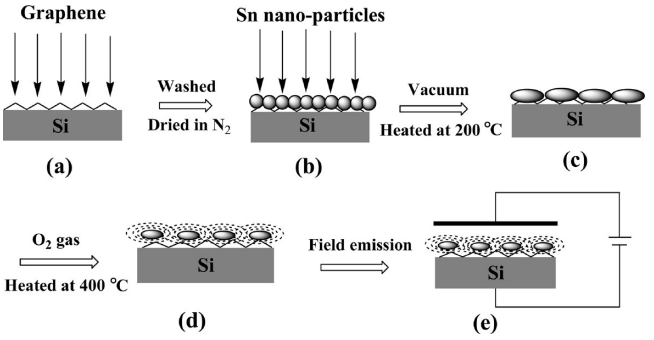

Figure 1. Schematic illustration of fabricating process of the G-SnO_2 composite nanostructures: (a) graphene was deposited on Si substrate; (b) Sn nanoparticles were sputtered on graphene-coated Si substrate, (c) formation of aggregated Sn droplets at 200 °C for 1 h, (d) formation of G-SnO_2 composite nanostructures at 400 °C under oxygen gas for 4 h, (e) schematic program of field emission evaluation.

electron-transport capability, and improve field-emission properties.

Moreover, photoluminescence (PL) is also one of the most fascinating properties of SnO_2 nanomaterials and has been extensively studied because of its importance in view of the optoelectronic devices, such as UV-light emitting diodes or laser diodes.[31,32] However, the PL of G-SnO_2 composite nanostructures are rarely reported.

In this paper, the SnO_2 nanostructures and G-SnO_2 composite nanostructures were prepared on n-Si (100) substrates. The crystal structures, morphology, field emission and PL of the SnO_2 nanostructures and G-SnO_2 composite nanostructures were analyzed by using X-ray diffraction (XRD, D/Max-2400), field-emission scanning electron microscope (FE-SEM; Hitachi S-4800), a computer-controlled power source with amperometer (Keithley 248), and fluorescence-phosphorescence spectrometer (LS-55), respectively.

2. EXPERIMENTAL METHODS

Schematic illustration of fabricating process of the G-SnO_2 composite nanostructures is shown in the Figure 1. The G-SnO_2 composite nanostructures were prepared on n-Si (100) substrates. The Si substrates were ultrasonically cleaned with acetone and alcohol in sequence for 15 min, then dipped into the diluted HF solution (5%) to remove a native oxide layer on them, and finally rinsed with distilled water and dried in nitrogen. In detail, graphene buffer layer were prepared on n-Si (100) substrates by electrophoretic deposition (EPD) technique (Figure 1a). Graphene (10 mg) and zinc nitrate hexahydrate (10 mg) were added to in 140 mL isopropyl alcohol solution and dispersed by sonication for 1 h, and then this homogeneous electrolyte was transferred into electrolytic cell system which was used to prepare the composite films. Platinum plate was mounted on the graphite anode, and a silicon wafer was mounted on the graphite cathode that was kept 10 mm away from the counter electrode. A DC voltage of 300 V was applied for 3 min to deposit graphene buffer layer on the Si substrates at 40 °C. After graphene-coated Si substrates were washed repeatedly with distilled water and ethanol, Sn nanoparticles were deposited using radio frequency (RF) reactive magnetron sputtering technique (Figure 1b). Before being loaded into the RF reaction chamber, the presample was dried in nitrogen. The Sn target (99.999% purity) was presputtered in pure Ar for 10 min to remove surface contamination and maintain system stability. The target-to-substrate distance was 50 mm. High-purity argon (99.99% purity) was used to act as the sputtering gas. The

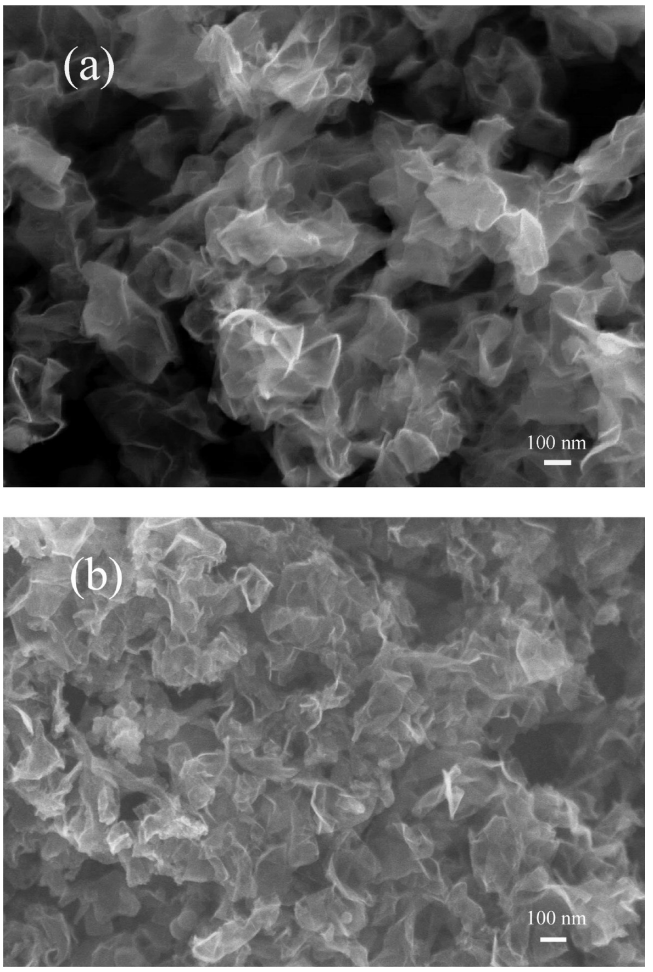

Figure 2. SEM images of (a) graphene prepared by arc discharge and (b) graphene deposited on the Si substrates by EPD technique.

base pressure of the system was 2×10^{-4} Pa and the deposition of Sn nanoparticles was carried out in the Ar atmosphere (20 sccm) at working pressure of 2.0 Pa. Sn nanoparticles were deposited on graphene-coated Si substrates at room temperature (RT) with RF power of 200 W used during sputtering for 5 and 10 min. A pretreatment step was preceded by increasing the temperature of the chamber rapidly up to 200 °C in vacuum for aggregating Sn droplets for 1 h (Figure 1c). After the pretreatment step, the temperature of the substrate was increased up to 400 °C and high-purity O_2 gas was introduced at flow rates of 20 sccm, for a period of 4 h (Figure 1d) to grow G-SnO_2 nanostructures. The SnO_2 nanostructures were prepared on n-Si (100) substrates under same condition by magnetron sputtering techniques. The mechanism involved here is a reaction between Sn and O_2 at high temperature. The reaction of $Sn + O_2 = SnO_2$ occurs at high temperature. After the growth period, the heated system was suddenly switched off and naturally cooled down to room temperature. Figure 1e shows schematic program of field emission evaluation.

The crystal structures of the SnO_2 nanostructures and G-SnO_2 composite nanostructures were analyzed by using X-ray diffraction (XRD, D/Max-2400) using the Cu Ka1 radiation with λ = 0.15406 nm. The morphology of the SnO_2 nanostructures and G-SnO_2 composite nanostructures were analyzed by using field-emission scanning electron microscope (FE-SEM; Hitachi S-4800). The field-emission characteristics of the SnO_2 nanostructures and G-SnO_2 composite nanostructures were estimated under base pressure 10^{-6} Pa at RT by using a computer-controlled power source with amperemeter

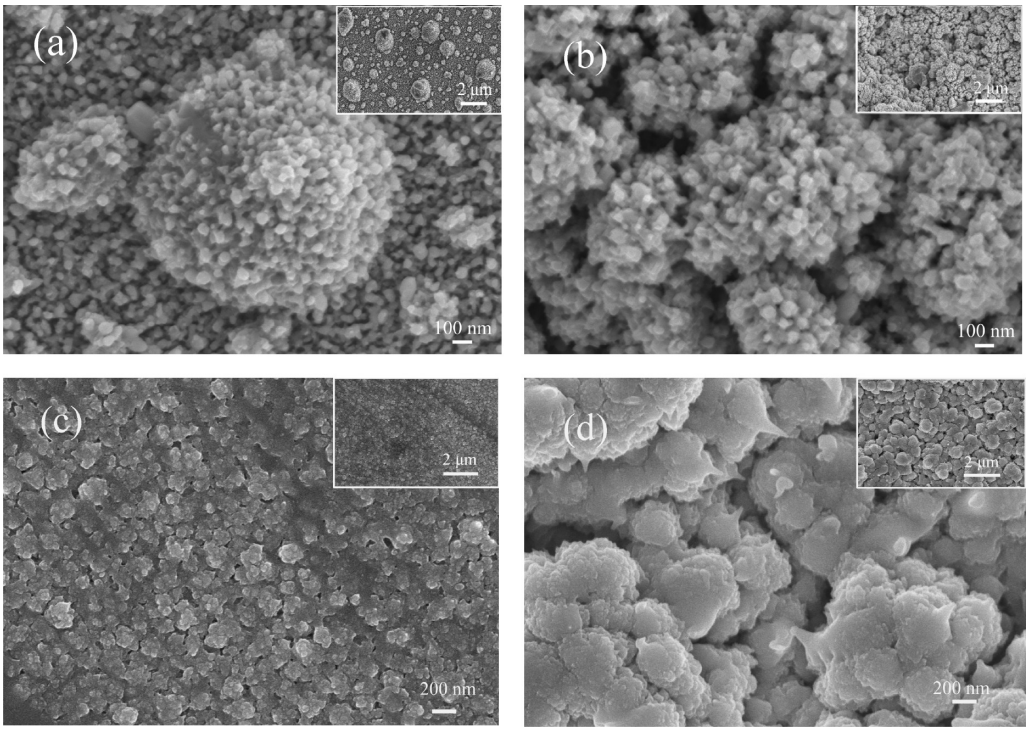

Figure 3. SEM images of the SnO_2 nanostructrues when sputtering time of Sn nanoparticles is (a) 10 and (c) 5 min and G-SnO_2 composite nanostructrues when sputtering time of Sn nanoparticles is (b) 10 and (d) 5 min. Their insets show the corresponding low magnification images.

(Keithley 248). A stainless-steel plate was used as the anode and the SnO_2 nanostructures or G-SnO_2 composite nanostructures were served as the cathode. The distance between the cathode and the anode was kept 300 μm, which was adjusted with a spiral micrometer before the measurements. The photoluminescence (PL) study was carried out on spectrometer (LS-55) whose excitation source was a Xe laser operating at 325 nm, and a 390 nm shortcut filter was used. The emitting light from the sample was focused into the entrance slit of a monochromator. This was picked up by photomultiplier tube. All the spectra measurements were performed in air at room temperature.

3. RESULTS AND DISCUSSIONS

Figure 2 shows SEM images of (a) graphene prepared by arc discharge and (b) graphene deposited on the Si substrates by EPD technique. Figure 2a shows the irregular morphology of the surface with exposed edge planes and the random expansive open areas, which is created by defects that arise from stress and hydrogen incorporation.[33] Similar graphene growth on the Si substrates by EPD technique is shown in Figure 2b, but it shows the more homogeneous layered platelets composed of curled nanosheets.

Figure 3 shows FE-SEM images of the SnO_2 nanostructrues when sputtering time of Sn nanoparticles is 10 min (a) and 5 min (c) and G-SnO_2 composite nanostructrues when sputtering time of Sn nanoparticles is 10 min (b) and 5 min (d). Their insets show the corresponding low magnification images. We can see that these images under higher magnification are assembled by different geometric sphere-flowers and each sphere-flower is composed of numerous nanorods protruding radially from center. In Figure 3a, it is clear that the shape of a few sphere-flowers is very different, and their locations are uneven and asymmetric on the Si substrates. It is interesting to see that the G-SnO_2 composite nanostructures are also grown in similar

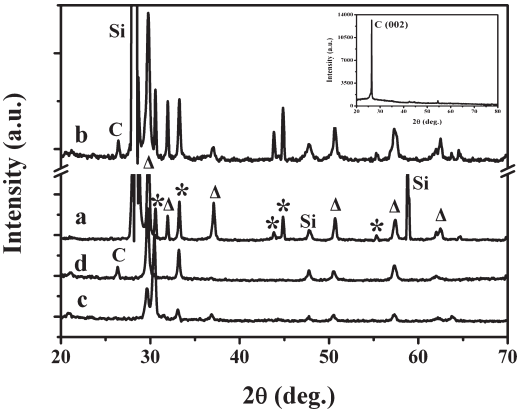

Figure 4. XRD spectra of the SnO_2 nanostructrues when sputtering time of Sn nanoparticles is (a) 10 and (c) 5 min and G-SnO_2 composite nanostructrues when sputtering time of Sn nanoparticles is (b) 10 and (d) 5 min. (* and **Δ** are designed to denote SnO_2 and Sn peaks, respectively). XRD spectra of graphene buffer layer are shown in the inset.

shapes that are clearly shown in the Figure 3b. However, these sphere-flowers are more uniform height along entire surface and more compact compared with SnO_2 nanostructures. Obviously, these distinct morphologies mainly result from the influence of graphene buffer layer during growth process of SnO_2, revealing that graphene acting as buffer layer of oxide composite nanostructures would affect the properties of the G-SnO_2 composite nanostructures. In comparison, as seen from Figure 3c, there are some small and compact droplets, while nanorods are not formed. Besides, although sphere-flowers are still formed after depositing graphene buffer layer, numerous nanorods protruding

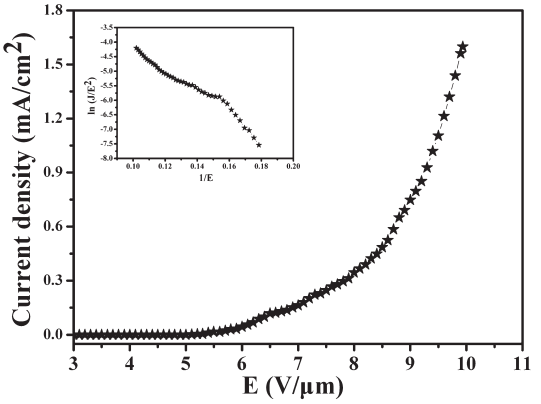

Figure 5. Field emission current density−field strength characteristics of graphene buffer layer by EPD. The corresponding F−N plot is shown in the inset.

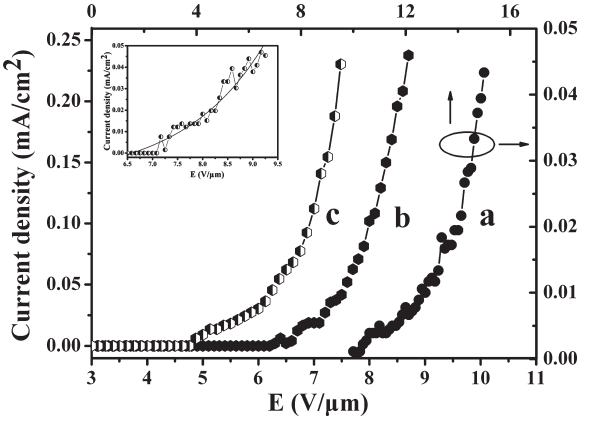

Figure 6. Field emission current density−field strength characteristics of the SnO_2 nanostructrues when sputtering time of Sn nanoparticles is (a) 10 and 5 min (inset) and G-SnO_2 composite nanostructrues when sputtering time of Sn nanoparticles is (b) 10 and (c) 5 min.

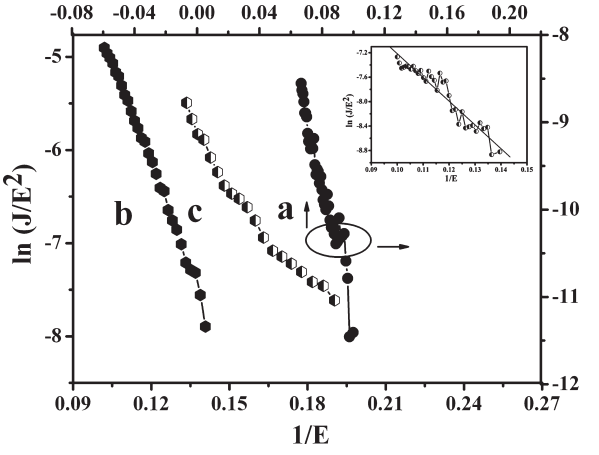

Figure 7. F−N plots of the SnO_2 nanostructrues when sputtering time of Sn nanoparticles is (a) 10 and 5 min (inset) and G-SnO_2 composite nanostructrues when sputtering time of Sn nanoparticles is (b) 10 and (c) 5 min.

radially from center are not formed completely (shown in the Figure 3d). This may be due to the deposited time of Sn nanoparticles is less than that in the Figure 3(b). It should also be mentioned that, SEM images show larger size because each sphere-flower is composed of numerous nanorods protruding radially from center.

Spectra a and c in Figure 4 show XRD patterns of SnO_2 nanostructures. The peaks at 29.75, 58.80, and 63.44° correspond to SnO_2 (111), (113), and (023) (JCPDS 29−1484), respectively. It confirms the diffraction signals are from SnO_2 nanostructures. Other diffraction peaks corresponding to Sn phases can also be observed, indicating that Sn droplets are not oxidized absolutely during the process of Figure 1d. The crystallite size of samples a, b, c, and d are 32.5, 26.9, 24.1, and 22.5 nm, respectively, calculated from Scherrer formula. There is a strong (002) diffraction peak in the XRD pattern of original graphene sheets as shown in the inset. It can be found that the interlayer spacing of the graphite ($2\theta_{(002)}$ = 26.42°) diffraction peak was 0.33706 nm, indicating that the graphite is approximate to natural graphene sheets ($d_{(002)}$ = 0.34 nm[34]), whereas for G-SnO_2 composite nanostructures (Figure 4b,d), the diffraction peak for graphene (002) is relatively low, indicating that significant face-to-face stacking is absent[35] because of the introduction of SnO_2 nanoparticles on the graphene sheets. In addition, as seen from Figure 4, strong Si diffraction peaks exist in the XRD patterns of SnO_2 nanostructrues and G-SnO_2 composite nanostructrues with the sputtering time of 10 min, whereas it cannot be detected from SnO_2 nanostructures and corresponding G-SnO_2 composite nanostructures with the decreased sputtering time of 5 min. In our syntheses, a heat-treatment at 200 °C under vacuum was employed to aggregate Sn nanoparticles into clusters. As seen from images a and b in Figure 3, small Sn nanoparticles can flow to aggregate large Sn droplets or cluster when the sputtering time of Sn nanoparticles is 10 min. As a result, the dispersion of Sn particles is not uniform. Thus, the thickness of final SnO_2 coating decreases in some regions. Therefore, strong Si diffraction peak will appear while X-ray scans these regions. On the contrary, when the sputtering time of Sn nanoparticles is 5 min, Sn nanoparticles can not flow to aggregate large Sn cluster due to the poor quantity of sputtered Sn. That is to say, the corresponding sample surfaces are more homogeneous and Si substrates are well covered. Therefore, there is no Si diffraction peak in the corresponding XRD patterns.

Figure 5 shows field emission current density−field strength characteristics of graphene buffer layer deposited on the Si substrates by EPD. The turn-on field E_{to}, defined as the field required at a current density of 1.0 μA/cm^2, of graphene buffer layer is 4.14 V/μm. The threshold field E_{thr}, defined as the field required at a current density of 1.0 mA/cm^2, of graphene buffer layer is 9.4 V/μm. The corresponding F−N plot is shown in the inset. The estimated field enhancement factor β is 979 and 2001 cm^{-1} for the graphene buffer layer at low and high field strength, respectively.

Figure 6 shows field emission current density−field strength characteristics of the SnO_2 nanostructrues when sputtering time of Sn nanoparticles is 10 min (a) and 5 min (inset) and G-SnO_2 composite nanostructrues when sputtering time of Sn nanoparticles is 10 min (b) and 5 min (c). When sputtering time of Sn nanoparticles is 10 min, E_{to} of SnO_2 nanostructures and G-SnO_2 composite nanostructures are 10.0 and 5.39 V/μm, and E_{thr} are 19.7 V/μm and 10.2 V/μm, respectively. When sputtering time of Sn nanoparticles is 5 min, E_{to} of SnO_2 nanostructures and G-SnO_2 composite nanostructures are 7.21 V/μm and 3.86 V/μm, and E_{thr} are 15.9 and 8.6 V/μm, respectively. This

Table 1. Key Performance Parameters of the Metal Oxide Field Emitters Reported in the Literature and This Work to Improve the Field-Emission Properties[a]

field emitters	E_{to} (V/μm)	E_{thr} (V/μm)	β (cm^{-1})	ref
SnO_2 film	9.33		874	2
SnO_2 nanorod arrays	1.67		2866	
SnO_2 NWs	6.5		2845	3
SnO_2:Sb NWs	4.9		3325	
SnO_2 NWs	(at 10 μA)			4
Before H_2 exposure	7.6			
After first H_2 exposure	6.9			
After second H_2 exposure	5.5			
ZnO:Al nanoarrays	0.5	10.8		5
ZnO:Al nanoarrays with ZnO buffer layer	<0.5	7		
ZnO:Al nanoarrays with Au film	<0.5	4.5		
SnO_2 nanostructures (10 min)	10.00	19.7	496	this work
G-SnO_2 composite nanostructures (10 min)	5.39	10.2	901	
G-SnO_2 composite nanostructures (5 min)	3.86	8.6	1787	

[a] The turn-on field and threshold field are at current densities of 1 $\mu A/cm^2$ and 1.0 mA/cm^2, respectively.

indicated that field emission of G-SnO_2 composite nanostructures was improved efficiently compared with the pure SnO_2 nanostructures. Recently, Hwang et al.[36] reported that there is a typical metal−semiconductor ohmic contact without a contact barrier between ZnO and graphene. Similarly, in our system, we deposited graphene on Si substrates to act as buffer layer. Because of high electron-transport and low contact barrier, the G-SnO_2 composite nanostructures show improved field emission properties. In addition, for G-SnO_2 composite nanostructures, E_{to} and E_{thr} decreased from 5.39 and 10.2 V/μm of the Sn nanoparticles sputtering time 10 min to 3.86 and 8.6 V/μm of the Sn nanoparticles sputtering time 5 min. These results indicated that in our system, with graphene acting as buffer layer, this effect on the field-emission properties of G-SnO_2 composite nanostructures is more obvious with decreasing the sputtering time of Sn nanoparticles to 5 min. It might be related to the decrease of the SnO_2 coating, which would be in favor of electron transport. However, the intrinsical mechanism is still unclear and further study is needed.

The field emission current density−field strength characteristics can be expressed by a simplified Fowler-Nordheim (F−N) equation[1]

$$J = \frac{A\beta^2 E^2}{\Phi} \exp\left(-\frac{B\Phi^{3/2}}{\beta E}\right) \quad (1)$$

The formula can be changed as following

$$\ln\left(\frac{J}{E^2}\right) = \ln\left(\frac{A\beta^2}{\Phi}\right) - \frac{B\Phi^{3/2}}{\beta}\frac{1}{E} \quad (2)$$

$$\beta = -\frac{6.83 \times 10^3 \Phi^{3/2}}{K}\ cm^{-1} \quad (3)$$

Where J is in the unit of mA/cm^2, E is in the unit of V/μm, Φ is the work function of the emitter, which is 4.5 eV for SnO_2.[37] $A = 1.54 \times 10^{-6}$ A eV V^{-2}, $B = 6.83 \times 10^9$ $eV^{3/2}$ V m^{-1}, and β is the field emission enhancement factor that is introduced to quantify the degree of enhancement of any tip over a flat surface, i.e., β represents the true value of the electric field at the tip compared to its average macroscopic value.[38]

Figure 7 shows F−N plots of the SnO_2 nanostructures and G-SnO_2 composite nanostructures corresponding to Figure 6. The F−N plots are basically a straight line, indicating that the field emission process from the SnO_2 nanostructures and G-SnO_2 composite nanostructures is a barrier tunneling, i.e., a quantum mechanical process.[1,39] From the slope K of $\ln(J/E^2) - 1/E$ plots, the field enhancement factor β of SnO_2 nanostructures and G-SnO_2 composite nanostructures is estimated. When sputtering time of Sn nanoparticles is 10 min, β of SnO_2 nanostructures and G-SnO_2 composite nanostructures are 496 cm^{-1} and 910 cm^{-1}, respectively. When sputtering time of Sn nanoparticles is 5 min, β of SnO_2 nanostructures and G-SnO_2 composite nanostructures are 1410 and 1787 cm^{-1}, respectively.

For comparison, Table 1 lists the key performance parameters of the metal oxide field emitters reported in the literature to improve the field emission properties by various approaches. One can see that field emission of our SnO_2 nanostructures is also improved largely by depositing graphene buffer layer. We found that the E_{to} value of the G-SnO_2 composite nanostructures at sputtering time of Sn nanoparticles 10 min is close to Sb doped SnO_2 NWs[3] and SnO_2 NWs after second H_2 exposure.[4] However, the amplitude variation in the E_{to} value of the G-SnO_2 composite nanostructures (10 min) compared with SnO_2 nanostructures (4.61 V/μm) is greater than that of SnO_2:Sb NWs compared with SnO_2 NWs (1.6 V/μm) and SnO_2 NWs after second H_2 exposure compared with SnO_2 NWs before H_2 exposure (2.1 V/μm). In addition, both the E_{to} value and the E_{thr} value are not low enough, compared with that of ZnO nanoarrays.[5] To our interesting, the amplitude variation of E_{thr} value of the G-SnO_2 composite nanostructures (10 min) compared with SnO_2 nanostructures (9.5 V/μm) is greater than that of ZnO:Al nanoarrays with ZnO buffer layer (3.8 V/μm) and with Au film compared with ZnO:Al nanoarrays (6.3 V/μm). So graphene can also be used as buffer layer acting as interface modification to effectively improve the field emission properties of SnO_2 nanostructures.

Figure 8 shows PL spectra of the SnO_2 nanostructrues when sputtering time of Sn nanoparticles is (a) 10 and (c) 5 min and G-SnO_2 composite nanostructrues when sputtering time of Sn nanoparticles is (b) 10 and (d) 5 min. Six strong emission bands

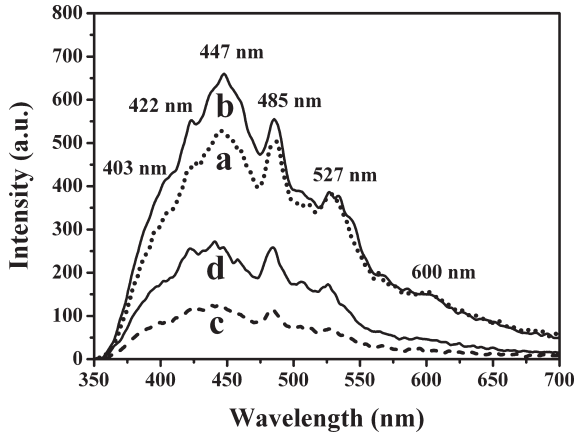

Figure 8. PL spectra of the SnO_2 nanostructrues when sputtering time of Sn nanoparticles is (a) 10 and (c) 5 min and G-SnO_2 composite nanostructrues when sputtering time of Sn nanoparticles is (b) 10 and (d) 5 min.

located at 403, 422, 447, 485, 527, and 600 nm were observed from PL spectra. Because the energy gap of the SnO_2 bulk is 3.62 eV, the band-to-band emission peak of the SnO_2 nanostructrues and G-SnO_2 composite nanostructures is not observed because of the limit of the PL detection range.[40] A similar result was also observed in the SnO_2 nanograss.[41] The intensity of six emission bands increased in the case of depositing graphene buffer layer at the same sputtering time of Sn nanoparticles compared with SnO_2 nanostructures, whereas PL intensity of G-SnO_2 composite nanostructures decreased as sputtering time of Sn nanoparticles decreased to 5 min. However, the position of six emission bands had no change after depositing graphene buffer layer or changing sputtering time of Sn nanoparticles.

Subsequently, we discussed the reason why the six emission bands can be formed in the PL spectra. In detail, the peak at 403 nm is independent of the concentration of oxygen vacancies, while it is from structural defects or luminescent centers, such as nanocrystals and defects in the SnO_2 film.[41] The peak at 447 nm is attributed to oxygen-related defects that have been introduced during the growth process.[42] The peak at 485 nm can be related to the 130° Sn coordinated surface oxygen vacancies.[32] The origin of the peak at 527 nm can be ascribed to the oxygen vacancies induced during film growth.[43] A similar mechanism is also reported in Al doped ZnO films.[44] The peak at 600 nm can be attributed to the SnO_2 emission band, which is related to the crystalline defects induced[45] during the formation process of the SnO_2 nanostructures and G-SnO_2 composite nanostructures. However, the peak at 422 nm is just found in our case. Kim et al.[40] reported that the peak position of the SnO_2 film does not change dramatically with decreasing temperature. They believed that the peak might be related to defects or nanocrystal grains or to defect levels associated with oxygen vacancies or Sn interstitials resulting from the nanosize of the SnO_2 film. So we believed that this peak at 422 nm may be caused by other defects or oxygen vacancies, and the detailed studies on the origin of the peak will be investigated in the future.

4. CONCLUSIONS

The SnO_2 nanostructures and G-SnO_2 composite nanostructures were prepared on n-Si (100) substrates. The E_{to} value of the G-SnO_2 composite nanostructures at sputtering time of Sn nanoparticles 10 min is close to Sb doped SnO_2 NWs and SnO_2 NWs after second H_2 exposure. Both the E_{to} value and the E_{thr} value are not low enough, compared with that of ZnO nanoarrays. However, the amplitude variation in E_{to} and E_{thr} values of the G-SnO_2 composite nanostructures at sputtering time of Sn nanoparticles 10 min after depositing graphene buffer layer is greater than those report in the literature mentioned. Six strong emission bands located at 403, 422, 447, 485, 527, and 600 nm were observed from PL spectra. The intensity of six emission bands increased in the case of depositing graphene buffer layer at the same sputtering time of Sn nanoparticles compared with SnO_2 nanostructures, whereas the PL intensity of G-SnO_2 composite nanostructures decreased as sputtering time of Sn nanoparticles decreased to 5 min. However, the position of six emission bands had no change after depositing graphene buffer layer or changing sputtering time of Sn nanoparticles. So graphene can also be used as buffer layer acting as interface modification to simultaneity improve the field emission and PL properties of SnO_2 nanostructures effectively.

AUTHOR INFORMATION

Corresponding Author

*Tel. & Fax: +86 931 4968055. E-mail: xbyan@licp.cas.cn.

ACKNOWLEDGMENT

This work was supported by the Top Hundred Talents Program of Chinese Academy of Sciences, the National Basic Research 973 Program of China, and the National Nature Science Foundations of China (Grants 51005225 and 51002161).

REFERENCES

(1) Chen, Y. J.; Li, Q. H.; Liang, Y. X.; Wang, T. H.; Zhao, Q.; Yu, D. P. *Appl. Phys. Lett.* **2004**, *85*, 5682–5684.
(2) Wang, X.; Liu, W.; Yang, H.; Li, X.; Li, N.; Shi, R.; Zhao, H.; Yu, J. *Acta Mater.* **2011**, *59*, 1291–1299.
(3) Wu, J. M. *Thin Solid Films* **2008**, *517*, 1289–1293.
(4) Jang, H. S.; Kang, S. O.; Kim, Y. I. *Solid State Commun.* **2006**, *140*, 495–499.
(5) Tang, H. P. *Doctoral Dissertation of Zhejiang University* **2006**, 74–76.
(6) Carey, J. D.; Smith, R. C.; Silva, S. R. P. *J. Mater. Sci.* **2006**, *17*, 405–412.
(7) Berger, C.; Song, Z.; Li, X. B.; Wu, X. S.; Brown, N.; Naud, C.; Mayou, D.; Li, T.; Hass, J.; Marchenkov, A. N.; Conrad, E. H.; First, P. N.; de Heer, W. A. *Science* **2006**, *312*, 1191–1196.
(8) Xu, T. G.; Zhang, L. W.; Cheng, H. Y.; Zhu, Y. F. *Appl. Catal., B* **2011**, *101*, 382–387.
(9) Zhang, S. L.; Zhang, Y. H.; Huang, S. P.; Qiao, L.; Yu, S. S.; Zheng, W. T. *J. Phys. Chem. C* **2011**, *115*, 9471–9476.
(10) Mai, Y. J.; Wang, X. L.; Xiang, J. Y.; Qiao, Y. Q.; Zhang, D.; Gu, C. D.; Tu, J. P. *Electrochim. Acta* **2011**, *56*, 2306–2311.
(11) Zhu, J. W.; Zeng, G. Y.; Nie, F. D.; Xu, X. M.; Chen, S.; Han, Q. F.; Wang, X. *Nanoscale* **2010**, *2*, 988–994.
(12) Li, N.; Wang, Z. Y.; Zhao, K. K.; Shi, Z. J.; Xu, S. K.; Gu, Z. N. *J. Nanosci. Nanotechnol.* **2010**, *10*, 6690–6693.
(13) Kim, H.; Seo, D. H.; Kim, S. W.; Kim, J.; Kang, K. *Carbon* **2011**, *49*, 326–332.
(14) Lu, T.; Zhang, Y. P.; Li, H. B.; Pan, L. K.; Li, Y. L.; Sun, Z. *Electrochim. Acta* **2010**, *55*, 4170–4173.
(15) Kim, Y. J.; Lee, J. H.; Yi, G. C. *Appl. Phys. Lett.* **2009**, *95* (213101), 1–3.
(16) Wu, J.; Shen, X. P.; Jiang, L.; Wang, K.; Chen, K. M. *Appl. Surf. Sci.* **2010**, *256*, 2826–2830.

(17) Wang, D. H.; Choi, D. W.; Li, J.; Yang, Z. G.; Nie, Z. M.; Kou, R.; Hu, D. H.; Wang, C. M.; Saraf, L. V.; Zhang, J. G.; Aksay, I. A.; Liu, J. *ACS Nano* **2009**, *3*, 907–914.
(18) Lambert, T. N.; Chavez, C. A.; Sanchez, B. H.; Lu, P.; Bell, N. S.; Ambrosini, A.; Friedman, T.; Boyle, T. J.; Wheeler, D. R.; Huber, D. L. *J. Phys. Chem. C* **2009**, *113*, 19812–19823.
(19) Williams, G.; Seger, B.; Kamat, P. V. *ACS Nano* **2008**, *2*, 1487–1491.
(20) Zhang, X. Y.; Li, H. P.; Cui, X. L.; Lin, Y. H. *J. Mater. Chem.* **2010**, *20*, 2801–2806.
(21) Kim, S. R.; Parvez, M. K.; Chhowalla, M. *Chem. Phys. Lett.* **2009**, *483*, 124–127.
(22) Yao, J.; Shen, X. P.; Wang, B.; Liu, H. K.; Wang, G. X. *Electrochem. Commun.* **2009**, *11*, 1849–1852.
(23) Lian, P .C.; Zhu, X. F.; Liang, S. Z.; Li, Z.; Yang, W. S.; Wang, H. H. *Electrochim. Acta* **2011**, *56*, 4532–4539.
(24) Paek, S. M.; Yoo, E. J.; Honma, I. *Nano Lett.* **2009**, *9*, 72–75.
(25) Wang, X. Y.; Zhou, X. F.; Yao, K.; Zhang, J. G.; Liu, Z. P. *Carbon* **2011**, *49*, 133–139.
(26) Zhang, L. S.; Jiang, L. Y.; Yan, H. J.; Wang, W. D.; Wang, W.; Song, W. G.; Guo, Y. G.; Wan, L. J. *J. Mater. Chem.* **2010**, *20*, 5462–5467.
(27) Du, Z. F.; Yin, X. M.; Zhang, M.; Hao, Q. Y.; Wang, Y. G.; Wang, T. H. *Mater. Lett.* **2010**, *64*, 2076–2079.
(28) Li, Y. M.; Lv, X. J.; Lu, J.; Li, J. H. *J. Phys. Chem. C* **2010**, *114*, 21770–21774.
(29) Wang, Z. Y.; Zhang, H.; Li, N.; Shi, Z. J.; Gu, Z. N.; Cao, G. P. *Nano Res.* **2010**, *3*, 748–756.
(30) Li, F.; Song, J.; Yang, H.; Gan, S.; Zhang, Q.; Han, D.; Ivaska, A.; Niu, L. *Nanotechnology* **2009**, *20* (455602), 1–4.
(31) Gaidi, M.; Hajjaji, A.; Smirani, R.; Bessais, B.; El Khakani, M. A. *J. Appl. Phys.* **2010**, *108* (063537), 1–5.
(32) Jean, S. T.; Her, Y. C. *J. Appl. Phys.* **2009**, *105* (024310), 1–6.
(33) Miller, J. R.; Outlaw, R. A.; Holloway, B. C. *Science* **2010**, *329*, 1637–1639.
(34) Wu, Y. P.; Wang, B.; Ma, Y. F.; Huang, Y.; Li, N.; Zhang, F.; Chen, Y. S. *Nano Res.* **2010**, *3*, 661–669.
(35) Yan, J.; Wei, T.; Qiao, W. M.; Shao, B.; Zhao, Q. K.; Zhang, L. J.; Fan, Z. J. *Electrochim. Acta* **2010**, *55*, 6973–6978.
(36) Hwang, J. O.; Lee, D. H.; Kim, J. Y.; Han, T. H.; Kim, B. H.; Park, M.; No, K.; Kim, S. O. *J. Mater. Chem.* **2011**, *21*, 3432–3437.
(37) Szuber, J.; Czempik, G.; Larciprete, R.; Adamowicz, B. *Sens. Actuators B* **2000**, *70*, 177–181.
(38) Yang, Y. H.; Wang, C. X.; Wang, B.; Xu, N. S.; Yang, G. W. *Chem. Phys. Lett.* **2005**, *403*, 248–251.
(39) Au, F. C. K.; Wang, K. W.; Tang, Y. H.; Zhang, Y. F.; Bello, I.; Lee, S. T. *Appl. Phys. Lett.* **1999**, *75*, 1700–1702.
(40) Kim, T. W.; Lee, D. U.; Yoon, Y. S. *J. Appl. Phys.* **2000**, *88*, 3759–3761.
(41) Wang, B.; Yang, Y. H.; Wang, C. X.; Xu, N. S.; Yang, G. W. *J. Appl. Phys.* **2005**, *98* (124303), 1–4.
(42) Her, Y. C.; Wu, J. Y.; Lin, Y. R.; Tsai, S. Y. *Appl. Phys. Lett.* **2006**, *89* (043115), 1–3.
(43) Zhu, Z.; Ma, J.; Luan, C. N.; Kong, L. Y.; Yu, Q. Q. *J. Lumin.* **2011**, *131*, 88–91.
(44) Ding, J. J.; Chen, H. X.; Zhao, X. G.; Ma, S. Y. *J. Phys. Chem. Solids* **2010**, *71*, 346–350.
(45) Wu, J. M. *J. Phys. Chem. C* **2008**, *112*, 13192–13199.